AGU ADVANCING EARTH AND SPACE SCIENCES

Radio Science

RESEARCH ARTICLE
10.1029/2024RS008192

Impact of Filtering Methods in the Assessment of COSMIC Electron Density Profiles Over the Brazilian Region: Excluding Profiles With Negative Values Is the Best Strategy?

Gabriel O. Jerez[1,2], **Manuel Hernández-Pajares**[2], **Daniele B. M. Alves**[1], and **João F. G. Monico**[1]

[1]Department of Cartography, São Paulo State University (UNESP), Presidente Prudente, São Paulo Brazil, [2]Department of Mathematics, Universitat Politècnica de Catalunya (UPC), UPC-IonSAT and UPC-IEEC Research Groups, Barcelona, Spain

Key Points:

- Proposal of filtering strategies for COSMIC profiles evaluated using 2-year data set close to solar maximum in low latitude
- Strategies assessed by profile exclusion rates and root mean square reduction for foF_2 and hmF_2, compared to ionosonde data
- Filtering based on a hmF_2 range of occurrence shown to be more effective compared to traditional filtering methods

Correspondence to:

G. O. Jerez,
gabriel.jerez@unesp.br

Citation:

Jerez, G. O., Hernández-Pajares, M., Alves, D. B. M., & Monico, J. F. G. (2025). Impact of filtering methods in the assessment of COSMIC electron density profiles over the Brazilian region: Excluding profiles with negative values is the best strategy? *Radio Science*, *60*, e2024RS008192. https://doi.org/10.1029/2024RS008192

Received 30 DEC 2024
Accepted 9 NOV 2025

Author Contributions:

Conceptualization: Gabriel O. Jerez, Manuel Hernández-Pajares
Formal analysis: Gabriel O. Jerez, Manuel Hernández-Pajares
Funding acquisition: Manuel Hernández-Pajares, Daniele B. M. Alves, João F. G. Monico
Investigation: Gabriel O. Jerez, Manuel Hernández-Pajares, Daniele B. M. Alves, João F. G. Monico
Methodology: Gabriel O. Jerez, Manuel Hernández-Pajares
Project administration: Daniele B. M. Alves
Resources: Gabriel O. Jerez, Manuel Hernández-Pajares, Daniele B. M. Alves, João F. G. Monico
Software: Gabriel O. Jerez
Supervision: Manuel Hernández-Pajares, Daniele B. M. Alves

Abstract Global Navigation Satellite Systems radio occultation (RO) is a valuable and relevant source of information from the atmosphere. Many efforts have been made to provide methods of validation of RO profiles, however, no clear methodology for filtering the profiles from RO can be easily found. In this study, we present strategies to filter RO electron density profiles over a low latitude region. Different methods are applied considering minimum values, manual filtering, hmF_2 range, and discrepancies with reference to the Chapman profile. The assessment is performed by means of ionosonde data for two years (2014–2015). The results show that assuming a minimum electron density limit slightly smaller than zero consistently with electron density estimation errors under very low actual values can provide significant improvements. In this study, the use of a -10^5 el/cm^3 limit led to better rates of retained profiles (65% vs. 32%) and a reduction in foF_2 root mean square (RMS) (12% vs. 7%) compared to the exclusion of all profiles with negative values. When considering only electron density values above 100 km in altitude, there is still a significant loss of about 20% in the number of profiles with the same reference values (84% vs. 63%), with a similar performance in the foF_2 RMS. The best performance is obtained with the strategies: hmF_2 range of occurrence (200–450 km) and the outliers identification (5 standard deviations limit), leading to a foF_2 RMS reduction of about 26% and 19%, and a hmF_2 RMS reduction of 34% and 25%, respectively, while keeping 91% and 82% of the original profiles.

Plain Language Summary Radio occultation (RO) is a method used for sounding the Earth's atmosphere. In the path between the Global Navigation Satellite Systems and the Low Earth Orbit satellite, the transmitted signal is influenced by the components of the atmosphere. With the RO it is possible to retrieve important parameters from the atmosphere and better understand its behavior. RO data is important because its data present a homogeneous distribution and can be used to complement several models, for example, the prediction of natural hazards. However, before using these profiles, it is important to validate them and develop methods for filtering, in order to avoid unreliable data. In this work, we present several ways of filtering RO ionospheric profiles considering a challenging region in low latitude, and data close to solar maximum. The data sets with the filtered profiles are assessed using ionosonde data as reference. For the scenarios considered, the best filtering strategies obtained are based on a hmF_2 range of occurrence and identification of outliers. The use of a negative minimum electron density limit performed better than a zero tolerance to negative values.

1. Introduction

Radio occultation (RO) is an important source of information from the atmosphere, including neutral and ionized layers. Since 1995, when the first RO mission was developed, GPS/Met (GPS-Meteorology), many other missions including receivers for RO have been launched, such as CHAMP (Challenging Minisatellite Payload), Gravity Recovery and Climate Experiment, SAC-C (Satélite de Aplicaciones Cientificas-C) and MetOp (Meteorological Operational satellite programe). Considering all the missions providing RO data, Constellation Observing System for Meteorology, Ionosphere and Climate (COSMIC/FORMOSAT-3) (2006–2020) has been one of the main ones, with a significant number of atmospheric profiles available, especially considering the ionosphere (R. A. Anthes et al., 2008). The COSMIC-2/FORMOSAT-7 mission, currently operational, in addition to providing a larger number of observations, also due to the use of other Global Navigation Satellite

Validation: Gabriel O. Jerez, Manuel Hernández-Pajares
Visualization: Gabriel O. Jerez, Daniele B. M. Alves, João F. G. Monico
Writing – original draft: Gabriel O. Jerez
Writing – review & editing: Gabriel O. Jerez

Systems (GNSS) constellations, is of special interest for the equatorial region because the configuration of the satellite orbits provides better coverage of this area (R. Anthes & Schreiner, 2019; Schreiner et al., 2020).

In addition to providing global coverage, because of the nature of the data acquisition, RO provides measurements that can help to suppress gaps from other techniques. In the last decades, several studies have been able to use RO data to investigate atmospheric phenomena (Arras et al., 2008; Coïsson et al., 2015; Hocke & Tsuda, 2001; Kursinski et al., 1997; Scherllin-Pirscher et al., 2021; Wickert et al., 2001) and assimilate it in atmospheric models, such as ionospheric (Hernández-Pajares et al., 1998; M. Angling & Cannon, 2004; Sai Gowtam & Tulasi Ram, 2017; Yao et al., 2018; dos Santos Prol et al., 2019; M. J. Angling et al., 2021) and numerical weather prediction (Buontempo et al., 2008; Cucurull & Purser, 2023; Healy et al., 2005; Lien et al., 2021; Ruston & Healy, 2021). The ionosphere is of special interest since it can influence the accuracy of GNSS and relates to several atmospheric dynamics. Many studies have shown that ionosphere impacts the transmission of radio signals, and consequently the GNSS positioning (Hernández-Pajares, Juan, & Sanz, 2000; Jerez et al., 2022; Lejeune et al., 2012; Orus Perez, 2017; Rovira-Garcia et al., 2020; dos Santos Prol et al., 2018). In this sense, many efforts have been made to use ionospheric information, including GNSS observation, to improve ionospheric models. Investigations have also shown that ionosphere relates to other atmospheric events, such as tsunamis and earthquakes, and ionospheric information can contribute in models to identify and predict the occurrence of such events (Astafyeva, 2019; Hickey et al., 2009; Komjathy et al., 2016; Tsai et al., 2011; Yang et al., 2019).

For the RO profiles retrieval, in general, the Abel inversion is applied (Fjeldbo et al., 1971; Hajj et al., 2002; Healy, 2001; Syndergaard, 1999). This inversion method assumes the spherical symmetry hypothesis, retrieving the electron density from the top to the bottom of the ionosphere in a recursive approach. This way, the errors in the electron density retrieval also propagates from the top, tending to accumulate in the bottom of the retrieved profile, in particular, when regions with strong horizontal ionospheric gradients are considered (García-Fernández et al., 2003; Lei et al., 2007; Schreiner et al., 1999; M. M. Shaikh et al., 2014). Many studies have been developed to investigate the impact of the spherical symmetry hypothesis as well as alternative ways to overcome this issue (Yue et al., 2010; Yue, Schreiner, and Kuo, 2013), including methods which resulted in new COSMIC products (Pedatella et al., 2015b). RO profiles from COSMIC (and from other RO missions) are available at the CDAAC (COSMIC Data Analysis and Archive Center) website (https://cdaac-www.cosmic.ucar.edu/).

In order to use ionospheric data from different sources for prediction purposes or any other investigation, validation and filtering are important processes, specially when such data is assumed as reference information. The geometry associated to the RO data acquisition, considering the GNSS and the Low Earth Orbit satellites, makes the validation of the RO profiles a challenge itself. However, the consistency and quality of the RO profiles must be considered in order to avoid noisy and not reliable information. In this sense, many efforts have been made to provide methods of validation of RO profiles. Considering electron density profiles, in general, comparisons with data from different missions (Chang et al., 2022; García-Fernández et al., 2003; Hernández-Pajares, Juan, Sanz, et al., 2000; Jin et al., 2019), models (Schreiner et al., 1999; Yue, Schreiner, Kuo, et al., 2013), ionosondes (Aa et al., 2016; Krankowski et al., 2011) and in situ measurements (Jakowski et al., 2003; Pedatella et al., 2015a) are used. A study has demonstrated that if the peak (NmF_2, hmF_2) of a retrieved electron density profile is coherent with a ground truth measurement, for instance, a co-located ionosonde, it can be expected that the topside of the retrieved profile can be considered accurate and, in some cases, able to be used as reference data for models validation purposes (M. Shaikh et al., 2018).

Besides the general assessment of RO missions, some strategies have been proposed to identify and exclude electron density profiles with questionable information. A method commonly used is to avoid negative values or to exclude complete profiles with negative electron density values, or with negative values above 100 km (Habarulema et al., 2021). It is worth highlighting that negative values below 100 km can result from the horizontal gradients and the assumption of spherical symmetry of atmosphere in the retrieval methods (Lei et al., 2007). In other words, to get a negative electron density in absolute value lower than the expected electron density retrieval error, may just indicate a very low actual electron density and it should not be a reason of rejection. Another approach used to identify problematic profiles is based on the peak height, excluding profiles with the peak occurrence out of a range, such as ∼200–450 km (Habarulema et al., 2021; Tulasi Ram et al., 2018). Also some statistic features can be used, such as the estimation of mean standard deviation threshold, using observations from other satellites collocated to the occultations being analyzed (Kuo-Feng et al., 2009). There are also filtering methods proposed for specific regions of ionosphere as the method presented in (Pignalberi et al., 2020) for the topside. However, as mentioned in Kuo-Feng et al. (2009), irregular behavior observed in the profiles can be related to physically meaningful ionospheric phenomena and not always corresponding to noisy or erroneous data. In this sense, the exclusion of profiles with negative values, for instance, may lead to the loss of important information and not necessarily exclude profiles with no reliable data. In this context, it is clear that there is still room for investigations of methods for filtering profiles from RO, specially considering regions under high influence of the ionosphere.

In this context, this study presents strategies for filtering electron density profiles from COSMIC mission, considering the general behavior of each profile. Different methods are applied considering manual filtering, minimum electron density values, hmF_2 range of occurrence, normal distribution and identification of outliers considering the discrepancies between values from RO and corresponding Chapman profiles. The study discusses different filtering methods, including already used and proposed strategies. All filtering methods are assessed by means of ionosonde data, applied for 2 years of data. In Section 2 we present the methods and strategies for the RO profiles filtering. Section 3 shows the data set and all the configurations adopted for the profiles assessment. Section 4 presents and discusses the impact of the filtering process in the assessment of electron density profiles from RO by means of ionosonde data. Section 5 contains the summary and conclusions.

2. RO Electron Density Profiles Filtering Methods

In this study, we present a manual and different automatic strategies to filter electron density profiles from RO based on the distribution of discrepancies between the original profiles and the corresponding Chapman model profiles. Five main filtering methods are presented: manual filtering, minimum electron density value, hmF_2 range of occurrence (Section 2.1), and two strategies considering the distribution of the discrepancies between the RO and the corresponding Chapman model profiles in a normal distribution and with the occurrence of outliers (Section 2.2).

2.1. Manual and Minimum Electron Density Filtering Strategies

The behavior of the ionosphere is irregular, especially considering the equatorial region, and specific areas such as the Brazilian sector. When assessing RO electron density profiles, it is worth highlighting that the geometry involved in the data acquisition with RO and the reference data, for instance an ionosonde, may be significantly different. In such a case the distance between the RO occurrence and the reference data may be even more relevant. This fact has motivated the proposal of this first filtering method, aiming to avoid profiles with indications of noisy data, coming from unreliable data or from ionospheric irregularities. This method aims to exclude profiles affected by intense ionospheric irregularities. Including such profiles could skew the mean error calculations when the ionospheric conditions at the RO measurement location differ significantly from those at the ionosonde, used as reference station.

The manual filtering is the only strategy discussed which is not an automatic process, consisting in analyzing each profile individually. In this filtering method, all the profiles have their data plotted with electron density values and corresponding altitudes. Then visually analyzing every plot, all the profiles with noisy, irregular or non-realistic behavior are excluded from the data set. Figure 1 presents examples of profiles excluded (top) and kept (bottom) for 1 January 2014. In this case, it is worth highlighting that, as shown in Figure 1, noisy values in the top and bottom areas are not considered for the exclusion of the profile. In general, the overall behavior of the electron density values are considered, especially in the region close to the peak. It is also worth it mentioning that, besides being a process which takes a lot of time to be done, it involves a level of subjectivity, since it depends on the judgment of the operator analyzing the profiles.

For the minimum electron density strategy, a minimum tolerance for electron density is defined. Then the profiles with electron density values smaller than the tolerance in any height are rejected. In this paper, besides the traditional use of zero (all profiles with negative values being excluded) as tolerance, we also use the value -10^5 el/cm^3 (corresponding to $-10^{11} el/m^3$). We also apply the same minimum limits considering only electron densities above 100 km. Another strategy used is the analysis of the peak height in a limited range of occurrence, in this study we exclude profiles with hmF_2 outside the range between 200 and 450 km.

10.1029/2024RS008192

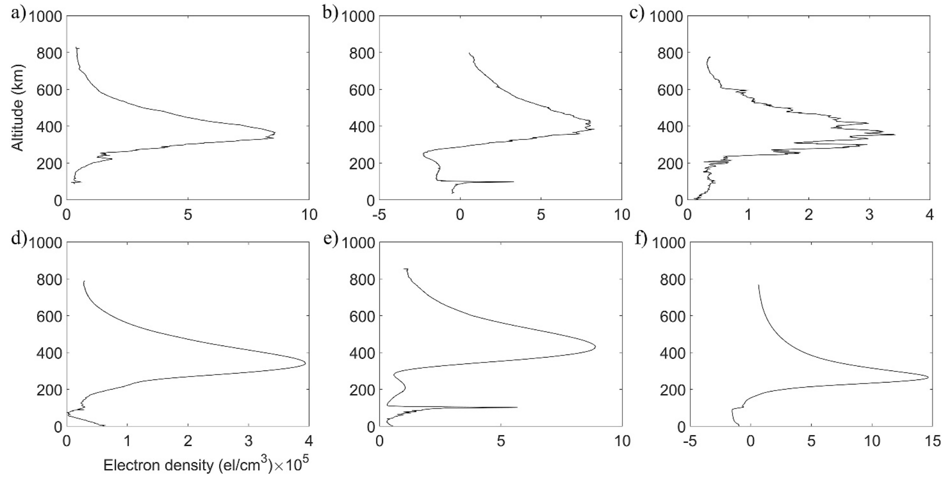

Figure 1. Profiles excluded (top) and kept (bottom) in the manual filtering process for 1 January 2014.

2.2. Filtering Based on the Normal Distribution and Outliers of the Discrepancies From Chapman Model Profiles

For the filtering methods related to Chapman model profiles (Chapman, 1931), we estimate a profile with the electron density (N) at a height (h) defined as:

$$N = NmF_2 \; e^{k(1-z-e^{-z})}, \tag{1}$$

where NmF_2 corresponds to the electron density peak at the F2 layer, $k = 1/2$ (Alpha-Chapman), and z is estimated as:

$$z = \frac{h - hmF_2}{H}, \tag{2}$$

with hmF_2 corresponding to the peak height at the $F2$ layer and H is the scale height. It should be mentioned that all the profiles are divided into two layers corresponding to approximate the E-layer (80–120 km) and F-layer (120 km–top). The initial filtering tests considered both layers, however the use of values from the E-layer led to the exclusion of almost all the profiles. In this sense, only the F-layer values are considered for the filtering strategies based on the Chapman profiles. The scale height estimation is obtained from Equations 1 and 2 in an iterative way as presented in (Olivares-Pulido et al., 2016), with z (reduced height) corresponding to:

$$z_{i+1} = 1 - e^{-z_i} - \frac{1}{k}\ln\frac{N}{N_m}. \tag{3}$$

with i corresponding to the index of the electron density value. For calculating H, four strategies are applied to define the Chapman model profile: for the first one the scale height used is the mean of the values obtained from the peak of the F2 layer to the top (MH); the second one takes into account the values from 50 km above the F2 layer peak to the top (MH+50); the third (VH) and fourth (VH+50) strategies follows the same idea, but considering a variable scale height, where the scale height at any given altitude is calculated using the 10 nearest data points in the ionospheric profile. In all cases, the equation presented by (Cappellari et al., 1976) is used as a first guess of the scale height (H), with hmF_2 representing the F2 layer peak height, both given in km:

$$H = \frac{5}{3}[30 + 0.2(hmF_2 - 200)]. \tag{4}$$

Figure 2 presents an example of a profile from 1 January 2014 considering the RO data (black) and the corresponding values from the Chapman profiles (a) and the differences considering the RO profile (b). In both plots, it

10.1029/2024RS008192

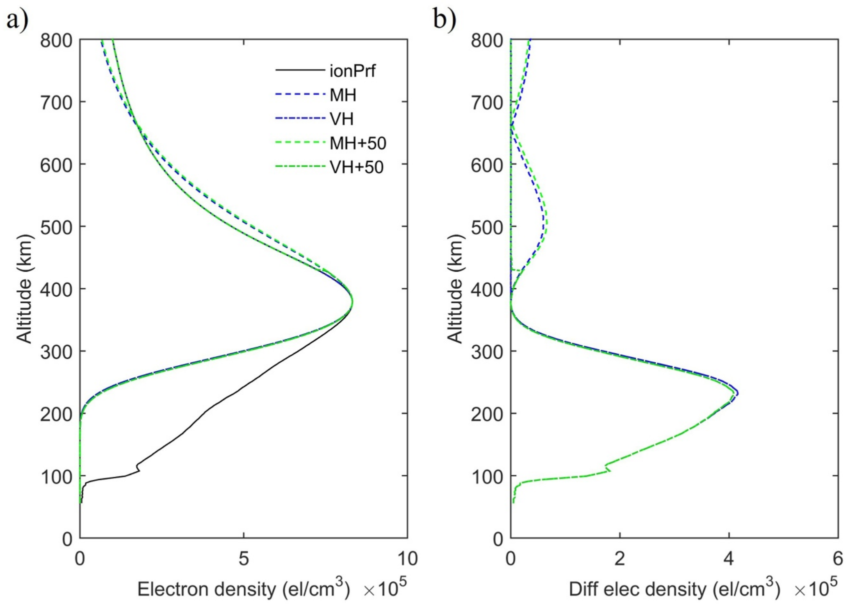

Figure 2. COSMIC profile from 1 January 2014 compared with the reconstruction of electron density profiles using Chapman model considering mean and variable H and values close to the peak.

is possible to notice that the use of a variable H has more influence on the estimated profile than the use of data close to the peak.

After the construction of the Chapman model profiles, the differences between electron density values from the RO and the Chapman model are calculated. Then, we analyze those differences to verify if its distribution is close to the Gaussian distribution. In other words, after calculating the mean discrepancies and corresponding standard deviations (STD), we use as a filtering condition the distribution of the differences assuming a normal distribution. We consider that the profiles present a normal distribution if the differences are inside the region corresponding to one standard deviation of the mean value for at least 68.27% of the cases. Then similar strategies are used for two standard deviation limits for 95.45% and three STD limit for 99.73% of the values.

The strategy considering the outliers is based on the same discrepancies from the Chapman model, but in this case the limit of STD is applied for the identification of outliers, here characterized as at least one discrepancy outside the limit defined by the mean and STD. For this study, we consider three different limits: three, four and five STD distances from the mean. Considering the conclusions presented with the comparison of the different ways of calculating the Chapman profiles, although the four options mentioned are applied, only the results considering a variable H are presented and discussed.

3. Data Set

In this study, electron density profiles from the COSMIC mission are analyzed for the years 2014 and 2015, which correspond to the peak of the solar cycle 24. The assessment is performed by means of ionosonde data from four stations of Instituto Nacional de Pesquisas Espaciais (INPE–Brazilian National Institute for Space Research) (Figure 3): BVJ03 located in Boa Vista-RR (2.8°N, 60.7°W; 12.9°N magnetic latitude), SAA0K in São Luiz-MA (2.5°S, 44.3°W; 0.8°S magnetic latitude), FZA0M in Fortaleza-CE (3.8°S, 38.5°W; 5.5°S magnetic latitude) and CAJ2M in Cachoeira Paulista-SP (22.7°S, 45.0°W; 16.4°S magnetic latitude). CAJ2M station is the only ionosonde in this study with less data, in 2014 only the last 31 days of data are available. Ionosonde data are available at the Space Weather Data Share, of Brazilian Study and Monitoring of Space Weather (EMBRACE/INPE) program (www2. inpe.br/climaespacial/portal/ionosondes-home/). For this study, only manual scaled foF_2 data are used to ensure the reliability of the reference data (see Araujo-Pradere et al. (2019)). The time resolution of the files is 10-min, and the time window limit applied is of 1 hr.

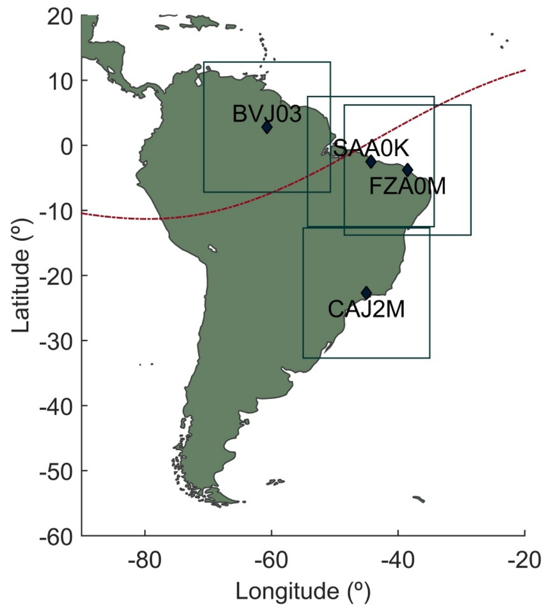

Figure 3. Location of the four ionosondes used for the profiles assessment and 20° search windows for each ionosondes position (blue).

For evaluation, the position of the ionosonde station is used as a reference for the window search, Figure 4 illustrates the assessment strategy. In this way, all the profiles with electron density peak occurrence inside the search window are analyzed. The assessment is performed considering the four ionosondes and three search windows: 5°, 10°, and 20° (in latitude and longitude). The largest search windows (20°) are presented in Figure 3 (blue windows) for each ionosonde. After the filtering based on the ionosondes positions, all the profiles in the corresponding region are filtered using the strategies previously mentioned in Section 2, leading to 30 filtering methods. However, as previously discussed, the methods that consider variable H (VH and VH+50) for the Chapman profile strategies resulted in profiles closer to the RO data, but the exclusion of values closer to the F2 peak (VH+50) does not influence the profile obtained. In this sense, in order to simplify the analysis, only the strategies based on the Chapman profile with variable H considering the values above the peak (VH), are presented. Table 1 shows the filtering strategies analyzed.

The analysis considers the root mean square (RMS) of the differences between the critical frequency, maximum electron density, and height peak at the F2 layer, from RO profiles and the corresponding values from the ionosondes. In addition to that, the RMS of the absolute and relative differences in shape function (SF) values, much more stable than the VTEC within the RO-affected region, are also analyzed (Hernández-Pajares, Juan, Sanz, et al., 2000):

$$SF(h) = \frac{N(LT, \Phi, h)}{VTEC(LT, \Phi)}, \tag{5}$$

where LT is the local time, Φ is the latitude and $VTEC$ is the vertical total electron content at a point with horizontal coordinates (LT, Φ). For the SF estimation, VTEC values from UQRG (UPC quarter-of-an-hour time resolution Rapid Global ionospheric maps) product are used (cddis.nasa.gov/archive/gnss/products/ionex/). The spatial resolution is 2.5° × 5°, in latitude and longitude, and the temporal resolution is 15 min.

4. Impact of Filtered Profiles in the Assessment of a RO Data Set

For the analysis, we considered the differences in the parameters of the peak of the F2 layer: foF_2, NmF_2, hmF_2, SF (SF), relative SF ($SF(\%)$); as well as the number of profiles kept and the mean distances from the corresponding occultations to the ionosondes. foF_2 and NmF_2 are also equivalent at L-band GNSS frequencies, so it was expected that these parameters would show similar behavior. In this sense, NmF_2 RMS is not presented here. Although significant differences can be found in some parameters, such as hmF_2, in general, they present a similar pattern related to which filtering mode leads to the best performance. Figure 5 presents the mean RMS obtained for the 2-year data and the four stations considering each search window. The results of manual filtering are suppressed from the analysis, as it led to a relatively small improvement (less than 8%) compared to the amount of profiles maintained (approximately 65%). It can be seen that, in general, filtering methods using outliers based on the Chapman profile and the three-standard deviation limit (O3+VH) and the range hmF_2 present the best performance considering foF_2 and SF, the good performance of the range hmF_2 is even more significant with hmF_2. The filtering method using the normal distribution based on the Chapman profile with 3 STD limit (N3+VH) presents the largest errors for most parameters, except for hmF_2, where the method excluding any profile with negative values leads to a worse performance (Ne_{min} 0). Figure 5 also shows that the number of profiles is significantly influenced by filtering methods, with the exclusion of more than 90% (N1+VH) of the profiles depending on the strategy applied. The mean

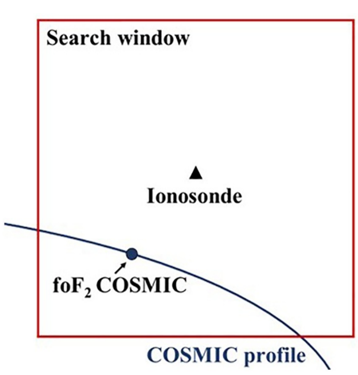

Figure 4. Assessment strategy by means of ionosonde data.

Table 1
Description of Filtering Modes

Mode	Description
Original	No filtering
Manual	Manual filtering
hmF_2	hmF_2 range interval between 200 and 450 km
$Ne_{\min}$ 0	Minimum electron density limit of 0 el/cm^3
$Ne_{\min} - 10^5$	Minimum electron density limit of -10^5 el/cm^3
$Ne_{\min}$ 0 >100	Minimum electron density limit of 0 el/cm^3 for altitudes above 100 km
$Ne_{\min} - 10^5 > 100$	Minimum electron density as -10^5 el/cm^3 for altitudes above 100 km
O3+VH	Outliers identification in a 3 STD limit of discrepancies between RO and Chapman profiles with variable H
O4+VH	Outliers identification in a 4 STD limit of discrepancies between RO and Chapman profiles with variable H
O5+VH	Outliers identification in a 5 STD limit of discrepancies between RO and Chapman profiles with variable H
N1+VH	Normal distribution in a 1 STD limit of discrepancies between RO and Chapman profiles with variable H
N2+VH	Normal distribution in a 2 STD limit of discrepancies between RO and Chapman profiles with variable H
N3+VH	Normal distribution in a 3 STD limit of discrepancies between RO and Chapman profiles with variable H

distances between the occultations and the ionosondes do not present significant changes with the different filtering methods, which indicates that the filtering strategies are not correlated with the region of occurrence of the occultations. In this way, considering that the general behavior of the error obtained for the selected parameters presents a similar performance, our main evaluation is based on the RMS obtained with foF_2 and hmF_2 differences between the COSMIC profiles and the ionosonde reference data, as well as the number of profiles kept in each filtering method.

Figure 6 presents a one-to-one representation between the RMS of the critical frequency (foF_2) and the number of profiles kept after the filtering methods, considering the four stations (BVJ03, SAA0K, FZA0M and CAJ2M) and the three search windows (5°, 10°, and 20°). It should be noted that the improvement in foF_2 RMS is not the only issue to be considered, but also the number of profiles filtered. For instance, the normal distribution with 1 STD (N1+VH) method, which presents one of the best performances for the 5° window, leads to a loss of more than

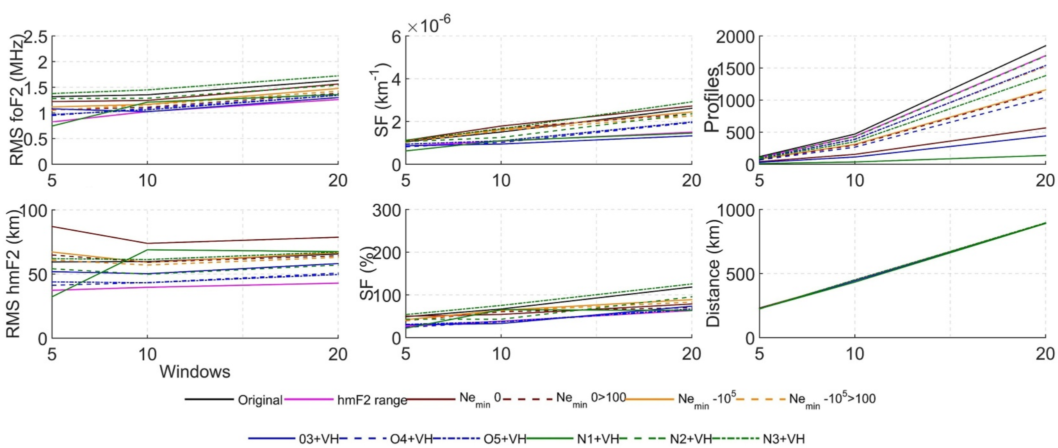

Figure 5. General performance of all filtering strategies considering foF_2, hmF_2, shape function, number of profiles and mean distance from the reference ionosonde.

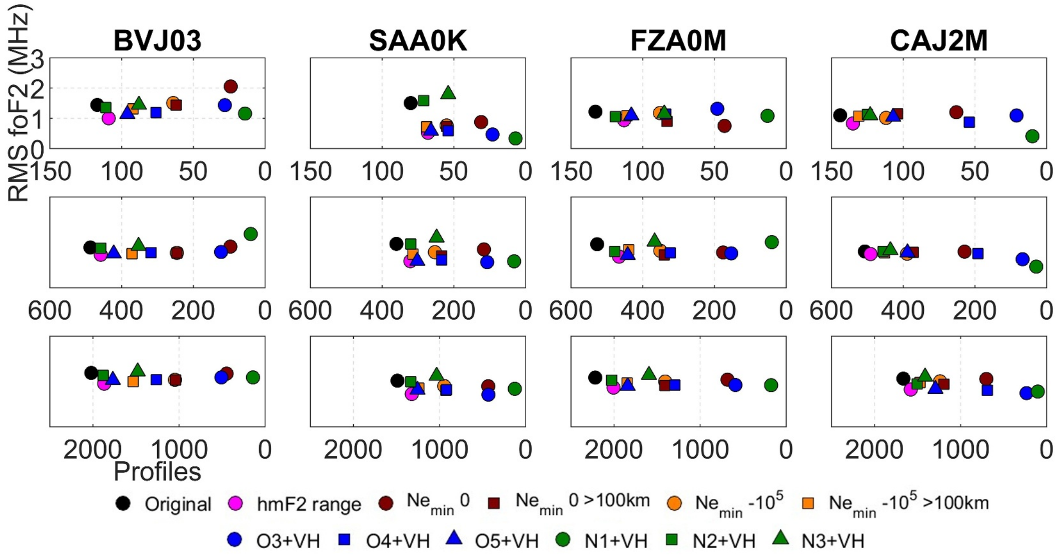

Figure 6. One-to-one representation of the root mean square of foF_2 differences and the number of profiles for all data sets for search windows with 5° (top), 10° (middle), and 20°(bottom), considering the four ionosondes (BVJ03, SAA0K, FZA0M, and CAJ2M) at the corresponding columns.

90% of the profiles, and the outliers identification with 3 STD limit (O3+VH) with one of the best performances for 10° and 20° windows, leads to a lost of more than 75% of the profiles. The figure also shows that some methods not only decrease the amount of profiles, but also increase the RMS obtained, such as the normal distribution with the 3 STD limit (N3+VH), which leads to a worse RMS and loss of almost 25% of the original profiles. Considering the number of profiles kept and the improvement in the foF_2 RMS, it is possible to identify the good performance of the peak height range (hmF_2 range) and the identification of outliers with 5 STD (O5+VH), with 26% and 19% improvement, respectively, while keeping 91% and 82% of the original profiles. The normal distribution with the 2 STD limit (N2+VH) maintains a significant number of profiles (90%), however, the improvement in foF_2 RMS is less than 5%. Only one filtering method presented mean foF_2 RMS values worse than the original data set, the use of the normal distribution with the 3 STD limit (N3+VH), with values up to 5% higher, and a loss of about 25% of the profiles.

Figure 7 presents a similar one-to-one representation but now with the RMS of the peak height (hmF_2) and the number of profiles kept after the filtering methods, considering the four stations (BVJ03, SAA0K, FZA0M, and CAJ2M) and the three search windows (5°, 10°, and 20°). Most of the behavior highlighted for foF_2 RMS can be observed for hmF_2 RMS. But in this case, not only N3+VH presented higher errors compared to the original data set. The normal distribution with 1 STD limit (N1+VH) and the minimum electron density limit presented worse RMS than the original data set for at least one of the three search windows. The zero tolerance for negative values in the entire profile (Ne_{min} 0) has the worst performance, with hmF_2 RMS 27% higher than the original data set, while keeping only 32% of the profiles. The best performance is obtained again by the filtering methods based on the peak height range (hmF_2 range) and the identification of outliers with 5 STD (O5+VH), with 34% and 24% improvement, respectively.

Summarizing the general performance with foF_2 RMS, Table 2 presents the mean RMS of the main filtering methods analyzed, relative to the original data set. Each line presents the relative performance of each filtering method with the percentage of profiles kept and the improvement in foF_2 RMS compared to the original data set. Taking into account all filtering methods and search windows, a mean of 40% of the profiles are eliminated, leading to an improvement of 11% in the foF_2 RMS. Although the mean percentage of profiles kept is similar for each search window (~60%), the mean improvement in the foF_2 RMS is inversely proportional to the size of the windows: ~13% (5°), ~11% (10°) and ~10% (20°). It can be verified that the peak height range (hmF_2 range) method leads to the best performance for the three search windows considered, with the foF_2 RMS improvements greater than 22%, while maintaining more than 89% of the original profiles.

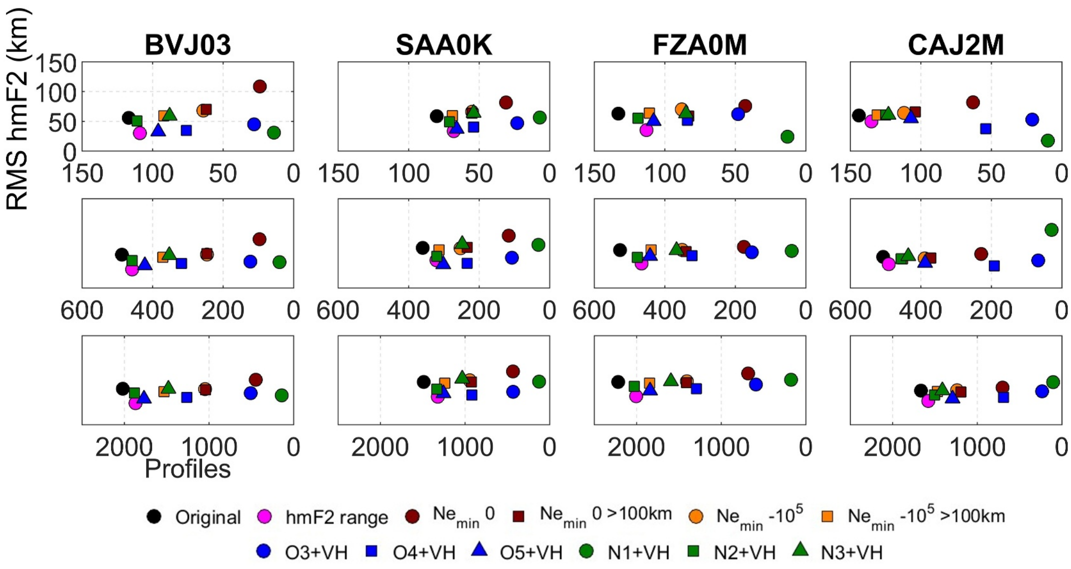

Figure 7. One-to-one representation of the root mean square of hmF_2 differences and the number of profiles for all data sets for search windows with 5° (top), 10° (middle), and 20°(bottom), considering the four ionosondes (BVJ03, SAA0K, FZA0M, and CAJ2M) at the corresponding columns.

Table 3 presents the mean hmF_2 RMS of the same filtering methods analyzed, relative to the original data set. Each line presents the relative performance of each filtering method with the percentage of profiles kept and the improvement in hmF_2 RMS compared to the original data set. In addition to the worse performance already mentioned for some of the filtering methods, especially those considering the normal distribution and minimum electron density profile limit, for the hmF_2 RMS, the general improvement is about 5% for all windows. The worst performance is observed with the zero minimum electron density limit ($Ne_{\min}$ 0) for the 5° window, where only 34% of the profiles are maintained and the RMS is 43% worse. The peak height range (hmF_2 range) method presented improvements of about 34% for all search windows.

We also investigated whether an elevated geomagnetic storm index could affect the performance of filtering methods. Figure 8 shows the results obtained with the main filtering methods for the four ionosondes, considering

Table 2
General Relative Performance in Percentage, Considering the Number of Profiles Kept and foF_2 Root Mean Square (RMS), Assuming as Reference the Original Data Set With 474 Profiles and foF_2 RMS of 1.30 MHz (for the 5°Window), 1,881 Profiles and foF_2 RMS of 1.35 MHz (for the 10°Window), and 7,391 Profiles and foF_2 RMS of 1.65 MHz (for the 20°Window)

Windows	5°		10°		20°	
Mode	Profiles kept (%)	RMS foF_2 (%)	Profiles kept (%)	RMS foF_2 (%)	Profiles kept (%)	RMS foF_2 (%)
hmF_2	89.66	32.95	92.29	22.81	91.67	22.04
$Ne_{\min}$ 0	33.97	5.80	32.85	9.40	30.65	4.49
$Ne_{\min} - 10^5$	67.30	12.01	65.87	13.69	62.77	9.83
$Ne_{\min}$ 0 > 100	64.14	15.62	63.37	17.34	61.83	15.40
$Ne_{\min} - 10^5 > 100$	85.02	15.89	83.79	13.66	82.41	12.82
O3+VH	25.32	7.76	23.92	21.73	23.87	17.28
O4+VH	56.54	21.61	56.73	18.42	56.39	16.07
O5+VH	79.54	21.11	82.62	20.27	83.30	16.93
N1+VH	9.28	29.85	7.50	0.60	7.39	15.73
N2+VH	89.87	2.98	91.02	5.62	91.31	5.46
N3+VH	73.84	−2.98	74.64	−5.84	74.73	−4.96

10.1029/2024RS008192

Table 3

General Relative Performance in Percentage, Considering the Number of Profiles Kept and foF_2 Root Mean Square (RMS), Assuming as Reference the Original Data set With 474 Profiles and hmF_2 RMS of 60 km (for the 5°Window), 1,881 Profiles and foF_2 RMS of 60 km (for the 10°Window), and 7,391 Profiles and foF_2 RMS of 66 km (for the 20°Window)

Windows	5°		10°		20°	
Mode	Profiles kept (%)	RMS hmF_2 (%)	Profiles kept (%)	RMS hmF_2 (%)	Profiles kept (%)	RMS hmF_2 (%)
hmF_2	89.66	34.31	92.29	33.69	91.67	34.81
Ne_{min} 0	33.97	−42.81	32.85	−20.05	30.65	−19.00
Ne_{min} $-$ 10^5	67.30	−12.39	65.87	0.89	62.77	−1.42
Ne_{min} $0 > 100$	64.14	−8.64	63.37	1.26	61.83	1.96
Ne_{min} $-$ $10^5 > 100$	85.02	−2.51	83.79	3.96	82.41	3.78
O3+VH	25.32	9.37	23.92	12.92	23.87	10.17
O4+VH	56.54	28.95	56.73	24.68	56.39	21.52
O5+VH	79.54	23.24	82.62	25.82	83.30	23.95
N1+VH	9.28	46.28	7.50	−15.34	7.39	−3.53
N2+VH	89.87	8.03	91.02	16.57	91.31	12.73
N3+VH	73.84	−3.47	74.64	−1.56	74.73	−1.57

the 5° search window, and the corresponding Kp (gray bars) index for each day. The results do not present any clear influence of larger Kp index with the larger differences in the foF_2 values. The same behavior can be observed for the other search windows (10° and 20°). Besides that, we also performed analysis considering only the foF_2 RMS from days with strong Kp ($Kp > 6$) and searched for correlations between the errors obtained and the corresponding Kp, but no clear influences could be added to this assessment. Considering the season of the year, no direct influence could be observed.

5. Summary and Conclusions

In this study, our objective was to analyze the impact of filtering strategies on the assessment of RO electron density profiles by means of ionosonde data. The study is carried out in the Brazilian region using data from 2014 to 2015. It should be noted that, in addition to being a challenging region when considering the ionospheric influence, the ionosonde stations used cover a large region, with distances from 660 to 3,310 km. The influence of the filtering process on the assessment of COSMIC electron density profiles is analyzed through 30 filtering

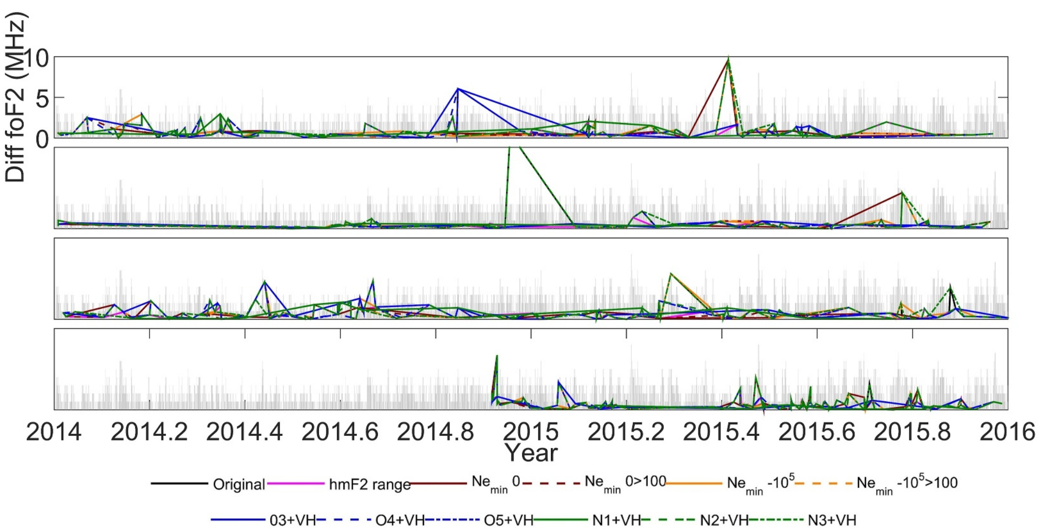

Figure 8. Differences of foF_2 compared to Kp index (gray bars) for search window with 5° for ionosondes BVJ03, SAA0K, FZA0M, and CAJ2M (from the top to the bottom).

methods. For the analysis, several parameters are considered, foF_2, NmF_2, hmF_2, SF difference (SF), relative SF difference (SF (%)), amount of profiles maintained and the mean distances from the occultations to the ionosondes. Since in general the parameters show similar behavior and the distance of profile occurrence is not directly influenced by the filtering process, foF_2, hmF_2 and the number of profiles kept are used in the evaluation.

Considering the simplest filtering methods, based on a minimum electron density limit, the use of a value lower than zero (in this study we use -10^5 el/cm^3) provides significant improvement in the rate of profiles kept (~65% against ~32%) and in the improvement in foF_2 RMS (12% against 7%). It is worth highlighting that, when assuming negative value as tolerance for the filtering method, we only refer to the decision on keeping or not the profiles. When using RO electron density profiles, no negative values should be considered in models or products. The use of the limits above 100 km leads to more profiles kept (84% and 63%), while no significant improvement is observed for the negative value limit, with foF_2 RMS improvements of 16% and 14%. The best performance for all the scenarios is obtained with the hmF_2 range, with 91% of the profiles kept, with rate of improvement of about 26% (foF_2 RMS) and 34% (hmF_2 RMS). The strategy considering the identification of outliers with the 5 STD limit also has good performance, with improvements of about 19% (foF_2 RMS) and 24% (hmF_2 RMS), while maintaining more than 81% of the original profiles. In general, the set of strategies that use the normal distribution leads to the worst performance in the assessment and, in some cases, to very high profiles exclusion rates (approximately 90% for N1+VH).

We reinforce that the conclusions here presented are based in measurements with occurrence in the Brazilian region (low latitude) in mid-high solar activity level. According to the scenario considered, the best strategy may be influenced, however, the season of the year does not seem to influence the performance of the methods presented in this study, as well as the geomagnetic activity (here represented by the Kp index). Taking into account the three search windows and the four ionosondes used for the assessment, we have shown general and specific analysis based on the different strategies. The simpler filtering method with most effective results is to apply the hmF_2 range of occurrence. Assuming the overall performances and the balance between improvement in the foF_2 RMS, hmF_2 RMS and the rates of profiles kept after the filtering process, the height peak range (hmF_2 range) and the outlier identification with a 5 STD limit (O5+VH) presented the best results and can be used in single or combined mode. In future studies, it is planned to expand this investigation generalizing the results on a global basis covering different solar activity levels.

Conflict of Interest

The authors declare no conflicts of interest relevant to this study.

Data Availability Statement

COSMIC data can be obtained at data.cosmic.ucar.edu/gnss-ro/cosmic1/postProc/level2/ (no registration required), UQRG products are available at cddis.nasa.gov/archive/gnss/products/ionex/ (registration required) and data from INPE Brazilian ionosondes can be found at embracedata.inpe.br/ionosonde/ (registration required).

Acknowledgments

We acknowledge University Corporation for Atmospheric Research (UCAR) for providing the COSMIC data and INPE for providing the ionosonde data. This study was financed in part by Fundação de Amparo à Pesquisa do Estado de São Paulo (FAPESP: 2021/05285-0 and 2022/00276-5). UPC-IonSAT also thanks the partial support of the PITHIA NRF EU project (Grant 101007599). We also acknowledge the National Institute of Science and Technology for GNSS in Support of Air Navigation (INCT GNSS-NavAer), funded by CNPq (465648/2014-2), FAPESP (2017/50115-0), and CAPES (88887.137186/2017-00). The Article Processing Charge for the publication of this research was funded by the Coordenação de Aperfeiçoamento de Pessoal de Nível Superior - Brasil (CAPES) (ROR identifier: 00x0ma614).

References

Aa, E., Liu, S., Huang, W., Shi, L., Gong, J., Chen, Y., et al. (2016). Regional 3-d ionospheric electron density specification on the basis of data assimilation of ground-based gnss and radio occultation data. *Space Weather*, *14*(6), 433–448. https://doi.org/10.1002/2016sw001363

Angling, M., & Cannon, P. (2004). Assimilation of radio occultation measurements into background ionospheric models. *Radio Science*, *39*(1), 1–11. https://doi.org/10.1029/2002rs002819

Angling, M. J., Nogués-Correig, O., Nguyen, V., Vetra-Carvalho, S., Bocquet, F.-X., Nordstrom, K., et al. (2021). Sensing the ionosphere with the spire radio occultation constellation. *Journal of Space Weather and Space Climate*, *11*, 56. https://doi.org/10.1051/swsc/2021040

Anthes, R., & Schreiner, W. (2019). Six new satellites watch the atmosphere over earth's equator. *Eos*, *100*. https://doi.org/10.1029/2019eo131779

Anthes, R. A., Bernhardt, P., Chen, Y., Cucurull, L., Dymond, K., Ector, D., et al. (2008). The cosmic/formosat-3 mission: Early results. *Bulletin of the American Meteorological Society*, *89*(3), 313–334. https://doi.org/10.1175/bams-89-3-313

Araujo-Pradere, E., Weatherhead, E., Dandenault, P., Bilitza, D., Wilkinson, P., Coker, C., et al. (2019). Critical issues in ionospheric data quality and implications for scientific studies. *Radio Science*, *54*(5), 440–454. https://doi.org/10.1029/2018rs006686

Arras, C., Wickert, J., Beyerle, G., Heise, S., Schmidt, T., & Jacobi, C. (2008). A global climatology of ionospheric irregularities derived from gps radio occultation. *Geophysical Research Letters*, *35*(14), L14809. https://doi.org/10.1029/2008gl034158

Astafyeva, E. (2019). Ionospheric detection of natural hazards. *Reviews of Geophysics*, *57*(4), 1265–1288. https://doi.org/10.1029/2019rg000668

Buontempo, C., Jupp, A., & Rennie, M. (2008). Operational nwp assimilation of gps radio occultation data. *Atmospheric Science Letters*, *9*(3), 129–133. https://doi.org/10.1002/asl.173

Cappellari, J., Vélez, C., & Fuchs, A. J. (1976). *Mathematical theory of the goddard trajectory determination system* (Vol. 71106). Goddard Space Flight Center.

Chang, H., Lee, J., Yoon, H., Morton, Y., & Saltman, A. (2022). Performance assessment of radio occultation data from geooptics by comparing with cosmic data. *Earth Planets and Space*, *74*(1), 1–17. https://doi.org/10.1186/s40623-022-01667-6

Chapman, S. (1931). The absorption and dissociative or ionizing effect of monochromatic radiation in an atmosphere on a rotating Earth. *Proceedings of the Physical Society*, *43*(1), 26–45. https://doi.org/10.1088/0959-5309/43/1/305

Coïsson, P., Lognonné, P., Walwer, D., & Rolland, L. M. (2015). First tsunami gravity wave detection in ionospheric radio occultation data. *Earth and Space Science*, *2*(5), 125–133. https://doi.org/10.1002/2014ea000054

Cucurull, L., & Purser, R. (2023). An improved one-dimensional bending angle forward operator for the assimilation of radio occultation profiles in the lower troposphere. *Monthly Weather Review*, *151*(5), 1093–1108. https://doi.org/10.1175/mwr-d-22-0073.1

dos Santos Prol, F., de Oliveira Camargo, P., Hernandez-Pajares, M., & Muella, M. T. d. A. H. (2018). A new method for ionospheric tomography and its assessment by ionosonde electron density, gps tec, and single-frequency ppp. *IEEE Transactions on Geoscience and Remote Sensing*, *57*(5), 2571–2582. https://doi.org/10.1109/tgrs.2018.2874974

dos Santos Prol, F., Themens, D. R., Hernández-Pajares, M., de Oliveira Camargo, P., & de Assis Honorato Muella, M. T. (2019). Linear vary-chap topside electron density model with topside sounder and radio-occultation data. *Surveys in Geophysics*, *40*(2), 277–293. https://doi.org/10.1007/s10712-019-09521-3

Fjeldbo, G., Kliore, A. J., & Eshleman, V. R. (1971). The neutral atmosphere of venus as studied with the mariner v radio occultation experiments. *Astronomical Journal*, *76*, 123. https://doi.org/10.1086/111096

García-Fernández, M., Hernandez-Pajares, M., Juan-Zornoza, J. M., & Sanz-Subirana, J. (2003). An improvement of retrieval techniques for ionospheric radio occultations. In *First CHAMP Mission results for gravity* (pp. 430–440). Magnetic and Atmospheric Studies.

Habarulema, J. B., Okoh, D., Burešová, D., Rabiu, B., Tshisaphungo, M., Kosch, M., et al. (2021). A global 3-d electron density reconstruction model based on radio occultation data and neural networks. *Journal of Atmospheric and Solar-Terrestrial Physics*, *221*, 105702. https://doi.org/10.1016/j.jastp.2021.105702

Hajj, G. A., Kursinski, E., Romans, L., Bertiger, W., & Leroy, S. (2002). A technical description of atmospheric sounding by gps occultation. *Journal of Atmospheric and Solar-Terrestrial Physics*, *64*(4), 451–469. https://doi.org/10.1016/s1364-6826(01)00114-6

Healy, S. (2001). Radio occultation bending angle and impact parameter errors caused by horizontal refractive index gradients in the troposphere: A simulation study. *Journal of Geophysical Research*, *106*(D11), 11875–11889. https://doi.org/10.1029/2001jd900050

Healy, S., Jupp, A., & Marquardt, C. (2005). Forecast impact experiment with gps radio occultation measurements. *Geophysical Research Letters*, *32*(3), L03804. https://doi.org/10.1029/2004gl020806

Hernández-Pajares, M., Juan, J., & Sanz, J. (2000). Improving the abel inversion by adding ground gps data to leo radio occultations in ionospheric sounding. *Geophysical Research Letters*, *27*(16), 2473–2476. https://doi.org/10.1029/2000gl000032

Hernández-Pajares, M., Juan, J., Sanz, J., & Colombo, O. L. (2000). Application of ionospheric tomography to real-time gps carrier-phase ambiguities resolution, at scales of 400–1000 km and with high geomagnetic activity. *Geophysical Research Letters*, *27*(13), 2009–2012. https://doi.org/10.1029/1999gl011239

Hernández-Pajares, M., Juan, J., Sanz, J., & Solé, J. (1998). Global observation of the ionospheric electronic response to solar events using ground and leo gps data. *Journal of Geophysical Research*, *103*(A9), 20789–20796. https://doi.org/10.1029/98ja01272

Hickey, M. P., Schubert, G., & Walterscheid, R. (2009). Propagation of tsunami-driven gravity waves into the thermosphere and ionosphere. *Journal of Geophysical Research*, *114*(A8), A08304. https://doi.org/10.1029/2009ja014105

Hocke, K., & Tsuda, T. (2001). Gravity waves and ionospheric irregularities over tropical convection zones observed by gps/met radio occultation. *Geophysical Research Letters*, *28*(14), 2815–2818. https://doi.org/10.1029/2001gl013076

Jakowski, N., Wehrenpfennig, A., Heise, S., Reigber, C., & Lühr, H. (2003). Status of ionospheric radio occultation champ data analysis and validation of higher level data products. In *First CHAMP Mission results for gravity* (pp. 462–472). Magnetic and Atmospheric Studies.

Jerez, G. O., Hernández-Pajares, M., Goss, A., da Silva, C. M., Alves, D. B., & Monico, J. F. (2022). Impact and synergies of gim error estimates on the vtec interpolation and single-frequency ppp at low latitude region. *GPS Solutions*, *26*(2), 40. https://doi.org/10.1007/s10291-022-01228-0

Jin, S., Gao, C., & Li, J. (2019). Atmospheric sounding from fengyun-3c gps radio occultation observations: First results and validation. *Advances in Meteorology*, *2019*, 1–13. https://doi.org/10.1155/2019/4780143

Komjathy, A., Yang, Y.-M., Meng, X., Verkhoglyadova, O., Mannucci, A. J., & Langley, R. B. (2016). Review and perspectives: Understanding natural-hazards-generated ionospheric perturbations using gps measurements and coupled modeling. *Radio Science*, *51*(7), 951–961. https://doi.org/10.1002/2015rs005910

Krankowski, A., Zakharenkova, I., Krypiak-Gregorczyk, A., Shagimuratov, I. I., & Wielgosz, P. (2011). Ionospheric electron density observed by formosat-3/cosmic over the european region and validated by ionosonde data. *Journal of Geodesy*, *85*(12), 949–964. https://doi.org/10.1007/s00190-011-0481-z

Kuo-Feng, Y., Chu, Y.-H., Su, C.-L., Ko, H.-T., & Wang, C.-Y. (2009). An examination of formosat-3/cosmic ionospheric electron density profile: Data quality criteria and comparisons with the iri model. *TAO: Terrestrial, Atmospheric and Oceanic Sciences*, *20*(1), 1.

Kursinski, E., Hajj, G., Schofield, J., Linfield, R., & Hardy, K. R. (1997). Observing earth's atmosphere with radio occultation measurements using the global positioning system. *Journal of Geophysical Research*, *102*(D19), 23429–23465. https://doi.org/10.1029/97jd01569

Lei, J., Syndergaard, S., Burns, A. G., Solomon, S. C., Wang, W., Zeng, Z., et al. (2007). Comparison of cosmic ionospheric measurements with ground-based observations and model predictions: Preliminary results. *Journal of Geophysical Research*, *112*(A7), A07308. https://doi.org/10.1029/2006ja012240

Lejeune, S., Wautelet, G., & Warnant, R. (2012). Ionospheric effects on relative positioning within a dense gps network. *GPS Solutions*, *16*(1), 105–116. https://doi.org/10.1007/s10291-011-0212-1

Lien, G.-Y., Lin, C.-H., Huang, Z.-M., Teng, W.-H., Chen, J.-H., Lin, C.-C., et al. (2021). Assimilation impact of early formosat-7/cosmic-2 gnss radio occultation data with taiwan's cwb global forecast system. *Monthly Weather Review*, *149*(7), 2171–2191. https://doi.org/10.1175/mwr-d-20-0267.1

Olivares-Pulido, G., Hernández-Pajares, M., Aragón-Àngel, A., & Garcia-Rigo, A. (2016). A linear scale height chapman model supported by gnss occultation measurements. *Journal of Geophysical Research: Space Physics*, *121*(8), 7932–7940. https://doi.org/10.1002/2016ja022337

Orus Perez, R. (2017). Ionospheric error contribution to gnss single-frequency navigation at the 2014 solar maximum. *Journal of Geodesy*, *91*(4), 397–407. https://doi.org/10.1007/s00190-016-0971-0

Pedatella, N., Yue, X., & Schreiner, W. (2015a). Comparison between gps radio occultation electron densities and in situ satellite observations. *Radio Science*, *50*(6), 518–525. https://doi.org/10.1002/2015rs005677

Pedatella, N., Yue, X., & Schreiner, W. (2015b). An improved inversion for formosat-3/cosmic ionosphere electron density profiles. *Journal of Geophysical Research: Space Physics*, *120*(10), 8942–8953. https://doi.org/10.1002/2015ja021704

Pignalberi, A., Pezzopane, M., Nava, B., & Coïsson, P. (2020). On the link between the topside ionospheric effective scale height and the plasma ambipolar diffusion, theory and preliminary results. *Scientific Reports*, *10*(1), 17541. https://doi.org/10.1038/s41598-020-73886-4

Rovira-Garcia, A., Ibáñez-Segura, D., Orús-Perez, R., Juan, J. M., Sanz, J., & González-Casado, G. (2020). Assessing the quality of ionospheric models through gnss positioning error: Methodology and results. *GPS Solutions*, *24*(1), 4. https://doi.org/10.1007/s10291-019-0918-z

Ruston, B., & Healy, S. (2021). Forecast impact of formosat-7/cosmic-2 gnss radio occultation measurements. *Atmospheric Science Letters*, *22*(3), e1019. https://doi.org/10.1002/asl.1019

Sai Gowtam, V., & Tulasi Ram, S. (2017). An artificial neural network-based ionospheric model to predict nmf2 and hmf2 using long-term data set of formosat-3/cosmic radio occultation observations: Preliminary results. *Journal of Geophysical Research: Space Physics*, *122*(11), 11743–11755. https://doi.org/10.1002/2017JA024795

Scherllin-Pirscher, B., Steiner, A. K., Anthes, R. A., Alexander, M. J., Alexander, S. P., Biondi, R., et al. (2021). Tropical temperature variability in the utls: New insights from gps radio occultation observations. *Journal of Climate*, *34*(8), 2813–2838. https://doi.org/10.1175/jcli-d-20-0385.1

Schreiner, W. S., Sokolovskiy, S. V., Rocken, C., & Hunt, D. C. (1999). Analysis and validation of gps/met radio occultation data in the ionosphere. *Radio Science*, *34*(4), 949–966. https://doi.org/10.1029/1999rs900034

Schreiner, W. S., Weiss, J., Anthes, R. A., Braun, J., Chu, V., Fong, J., et al. (2020). Cosmic-2 radio occultation constellation: First results. *Geophysical Research Letters*, *47*(4), e2019GL086841. https://doi.org/10.1029/2019gl086841

Shaikh, M., Nava, B., & Haralambous, H. (2018). On the use of topside ro-derived electron density for model validation. *Journal of Geophysical Research: Space Physics*, *123*(5), 3943–3954. https://doi.org/10.1029/2017ja025132

Shaikh, M. M., Notarpietro, R., & Nava, B. (2014). The impact of spherical symmetry assumption on radio occultation data inversion in the ionosphere: An assessment study. *Advances in Space Research*, *53*(4), 599–608. https://doi.org/10.1016/j.asr.2013.10.025

Syndergaard, S. (1999). *Retrieval analysis and methodologies in atmospheric limb sounding using the gnss radio occultation technique* (Vol. 99). Danish Meteorological Institute.

Tsai, H.-F., Liu, J.-Y., Lin, C.-H., & Chen, C.-H. (2011). Tracking the epicenter and the tsunami origin with gps ionosphere observation. *Earth Planets and Space*, *63*(7), 859–862. https://doi.org/10.5047/eps.2011.06.024

Tulasi Ram, S., Sai Gowtam, V., Mitra, A., & Reinisch, B. (2018). The improved two-dimensional artificial neural network-based ionospheric model (annim). *Journal of Geophysical Research: Space Physics*, *123*(7), 5807–5820. https://doi.org/10.1029/2018ja025559

Wickert, J., Reigber, C., Beyerle, G., König, R., Marquardt, C., Schmidt, T., et al. (2001). Atmosphere sounding by gps radio occultation: First results from champ. *Geophysical Research Letters*, *28*(17), 3263–3266. https://doi.org/10.1029/2001gl013117

Yang, H., Monte Moreno, E., & Hernández-Pajares, M. (2019). Addtid: An alternative tool for studying earthquake/tsunami signatures in the ionosphere. case of the 2011 tohoku earthquake. *Remote Sensing*, *11*(16), 1894. https://doi.org/10.3390/rs11161894

Yao, Y., Liu, L., Kong, J., & Zhai, C. (2018). Global ionospheric modeling based on multi-gnss, satellite altimetry, and formosat-3/cosmic data. *GPS Solutions*, *22*(4), 1–12. https://doi.org/10.1007/s10291-018-0770-6

Yue, X., Schreiner, W. S., & Kuo, Y.-H. (2013). Evaluating the effect of the global ionospheric map on aiding retrieval of radio occultation electron density profiles. *GPS Solutions*, *17*(3), 327–335. https://doi.org/10.1007/s10291-012-0281-9

Yue, X., Schreiner, W. S., Kuo, Y.-H., Wu, Q., Deng, Y., & Wang, W. (2013b). Gnss radio occultation (ro) derived electron density quality in high latitude and polar region: Ncar-tiegcm simulation and real data evaluation. *Journal of Atmospheric and Solar-Terrestrial Physics*, *98*, 39–49. https://doi.org/10.1016/j.jastp.2013.03.009

Yue, X., Schreiner, W. S., Lei, J., Sokolovskiy, S. V., Rocken, C., Hunt, D. C., & Kuo, Y.-H. (2010). Error analysis of abel retrieved electron density profiles from radio occultation measurements. *Annales Geophysicae*, *28*(1), 217–222. https://doi.org/10.5194/angeo-28-217-2010